Slow electrons impinging on dielectric solids. I. Basic aspects

Maurizio Dapor
INFM and Centro Materiali e Biofisica Medica, Istituto Trentino di Cultura, I-38050 Povo, Trento, Italy

Antonio Miotello
INFM and Dipartimento di Fisica dell'Università di Trento, I-38050 Povo, Trento, Italy

(Received 2 December 1996; revised manuscript received 18 February 1997)

The basic aspects related to the scattering processes, useful for both the analytical and Monte Carlo calculation of backscattering and the depth distribution of low-energy ($E_0 \leqslant 10$ keV) electrons impinging on solid targets, are described. After a careful analysis of the scattering mechanisms, selected new results regarding elastic and inelastic scattering of low-energy electrons impinging on SiO_2 are reported. Comparison with experimental data and earlier theoretical results show a general good agreement. [S0163-1829(97)05128-X]

I. INTRODUCTION

Dielectric materials, namely biological materials, ceramics, glasses, microelectronic devices and so on, exhibit charging effects when irradiated with electrons. Electron irradiation is widely utilized in microanalytical techniques such as Auger electron spectroscopy, transmission electron microscopy, electron-probe microanalysis, and electron-beam lithography.

The analysis of charging phenomena was already reported in the literature[1–4] and macroscopic equations were utilized to compute electric charge distribution, electric fields, and the surface electrical potential. However, in these approaches, the microscopic details were not investigated; only in one case[1] the dynamics of the injected charges, along with charge-recombination processes, were considered.

In this paper and in the following[5] we address, both at a microscopic and macroscopic level, problems connected to the charge injection into insulating materials, and show that, at an atomic level, relevant problems are still open questions which merit deeper investigations than those reported in the quoted literature.

The study of charging phenomena implies the knowledge of (1) the depth distribution of the implanted electrons, or the implantation profile; (2) the amount of the emitted secondary electrons to make the appropriate charge balance in evaluating the induced electric fields and surface electric potential; (3) and the dynamics of the charge-recombination processes to evaluate the conditions to avoid dielectric breakdown.

The absorbed electrons, indeed, represent the charge source term for the continuity equation in the ordinary and electric-field-assisted diffusion process. The surface electric field and potential are computable once the diffusion processes are established. Then we describe here the basic aspects related to a theoretical (Monte Carlo) calculation of the depth distribution and of the backscattering coefficient for low-energy ($E_0 \leqslant 10$ keV) electrons bombarding insulating materials such as Al_2O_3 and SiO_2.

In the following paper[5] we will compute the depth-distribution function of the primary electrons, which will be used to solve the macroscopic electric-field-assisted diffusion equation. It permits the evaluation of the surface electric potential, a key parameter determining the shifts of Auger lines due to charging effects during Auger analysis of insulating materials.

II. THEORETICAL FRAMEWORK

Excellent reviews about the subject of electron-solid interaction have been given, for example, by Niedrig,[6] Goldstein *et al.*,[7] Newbury *et al.*,[8] Feldman and Mayer,[9] and Messina *et al.*[10] Here, it is worth analyzing some general aspects of the problem of the interaction of electrons with solid targets to critically establish the fundamentals of the Monte Carlo calculations.

When an electron beam impinges on a solid target, some electrons, after a number of elastic and inelastic collisions with the atoms of the target, come back and emerge from the surface, while some other electrons are transmitted and emerge from the back of the sample. The remaining electrons are trapped in the target. The fractions of absorbed, backscattered, and transmitted electrons depend on the thickness of the target.

When the target is a bulk, the fraction of backscattered electrons reaches its saturation value, generally called the backscattering coefficient, hereafter indicated with η. Then, it is possible to define a thickness R so that, for each thickness greater than R, the fraction of transmitted electrons is zero and that of the reflected ones is equal to η. The quantity R is generally known as the maximum penetration range. Both R and η depend on the primary energy E_0 of the electron beam and on the atomic and electronic structure of the irradiated material.

In order to describe the processes that occur during the implantation of the primary electrons in the insulating material, we need to know the elastic[11–34] and inelastic[35–61] processes suffered by the electrons traveling in the solid target. Indeed, in each collisional event with an atomic electron or a nucleus, the incident electron both loses energy and changes its travelling direction. The energy dissipation of the incident electron mainly occurs through atomic electron excitation or ejection and plasmon excitation. These scattering processes also influence the electron trajectory in the solid, but only weakly. The nuclear collisions, on the other hand, due to the

large mass difference between the electron and the atomic nucleus, are nearly elastic: they strongly affect the direction of the incident electron in the solid without substantial energy transfer.

The differential elastic-scattering cross section of electrons interacting with free and bound atoms, particularly for low-medium kinetic energy, is not computable by using simple analytical formulas, but numerical quantum mechanical calculations are generally necessary. The inelastic events can be described by the inelastic mean free path, and, in the continuous-slowing-down approximation, by the stopping power, viz., the mean energy loss per unit distance traveled by the electron inside the solid.

A. Elastic scattering

1. Mott cross section

The elastic scattering process can be treated by calculating the phase shifts.[11–14] Since the large-r asymptotic behavior (r is the radial coordinate) of the radial wave function is known, the phase shifts can be computed by solving the Dirac's equation for a central electrostatic field up to a large radius where the atomic potential can be safely neglected.

When the atom is bound in a solid, the interaction potential between the electron and the atom is different from the interaction potential between the electron and the free atom. This is due to the atomic configuration in the solid in which the outer electronic orbitals of the atoms are modified. In order to take into account such changes, solid-state effects can be introduced by using the muffin-tin potential in which the potential of each atom of the solid is altered by the nearest-neighbor atoms.

The differential elastic-scattering cross section is given by

$$\frac{d\sigma}{d\Omega}=|f|^2+|g|^2, \tag{1}$$

where the direct and spin-flip scattering amplitudes $f(\theta)$ and $g(\theta)$ (θ=the scattering angle with respect to the incidence direction) are given by[11,14]

$$f(\theta)=\frac{1}{2iK}\sum_{l=0}^{\infty}\{(l+1)[\exp(2i\delta_l^-)-1] + l[\exp(2i\delta_l^+)-1]\}P_l(\cos\theta), \tag{2}$$

$$g(\theta)=\frac{1}{2iK}\sum_{l=1}^{\infty}[-\exp(2i\delta_l^-)+\exp(2i\delta_l^+)]P_l^1(\cos\theta). \tag{3}$$

In these equations, $K^2=(E^2-m^2c^4)/\hbar^2c^2$, $\hbar K$ is the momentum of the electron, E the total energy, m the electron mass, c the speed of light, P_l are the Legendre's polynomials, and

$$P_l^1(x)=(1-x^2)^{1/2}\frac{dP_l(x)}{dx}. \tag{4}$$

The phase shifts δ_l^- and δ_l^+ can be computed by using the equation (see, for example, Refs. 23,26,32,34)

$$\tan\delta_l^{\pm}=\frac{Kj_{l+1}(Kr)-j_l(Kr)[\zeta\tan\phi_l^{\pm}+(1+l+k^{\pm})/r]}{Kn_{l+1}(Kr)-n_l(Kr)[\zeta\tan\phi_l^{\pm}+(1+l+k^{\pm})/r]}, \tag{5}$$

where

$$\zeta=\frac{E+mc^2}{\hbar c}. \tag{6}$$

In equation (5), $k^+=-l-1$, and $k^-=l$, j_l are the regular spherical Bessel functions, n_l the irregular spherical Bessel functions, and

$$\phi_l^{\pm}=\lim_{r\to\infty}\phi_l^{\pm}(r), \tag{7}$$

where $\phi_l^{\pm}(r)$ is the solution of the Dirac's equation which can be reduced, as shown by Lin, Sherman, and Percus[12] and by Bunyan and Schonfelder,[13] to the first-order differential equation:

$$\frac{d\phi_l^{\pm}(r)}{dr}=\frac{k^{\pm}}{r}\sin[2\phi_l^{\pm}(r)]-\frac{mc^2}{\hbar c}\cos[2\phi_l^{\pm}(r)]+\frac{E-V(r)}{\hbar c}. \tag{8}$$

Here, $V(r)$ is the electron-atom potential.

2. The atomic potential

To calculate the electron-atom potential, for atomic number Z greater than 18, the Dirac-Hartree-Fock-Slater field should be used, while it is preferable to use the Hartree-Fock field for atomic numbers lower than 19. The nonrelativistic fields, indeed, are realistic where the relativistic effects are small and the LS angular momentum coupling is adequate.

Moreover, in order to reduce the computer calculation time, the analytical approximation proposed by Cox and Bonham[62] for the Hartree-Fock field and that of Salvat *et al.*[63] for the Dirac-Hartree-Fock-Slater field can be utilized. The corresponding atomic potential takes the form of a superposition of Yukawa's potentials which depend on a number of parameters. Such parameters have been determined by analytical fitting of self-consistent fields and can be found in Refs. 62,63.

The atomic potential is generally expressed by a pure Coulomb potential multiplied by a dimensionless function which approximates the screening of the nucleus by the orbital electrons, i.e., the atomic screening function $\psi(r)$. In other words, the atomic screening function is defined as the ratio between the electrostatic potential experienced by a point charge at a distance r from the nucleus and the electrostatic potential of the bare nucleus (assuming spherical symmetry). The atomic screening functions of Cox and Bonham[62] and of Salvat *et al.*[63] are given by

$$\psi(r)=\sum_{i=1}^{p}A_i\exp(-\alpha_i r), \tag{9}$$

where p, A_i, and α_i depend on the element and on the authors. Expression (9) has the analytical form originally proposed by Molière in order to approximate the Thomas-Fermi differential equation.

3. Electron exchange

Since electrons are identical particles, exchange effect should be taken into account when low-energy elastic scattering is treated; indeed, the incident electron may be captured by an atom with emission of a new electron. Exchange effects can be described by adding the Furness and McCarthy[64] expression to the electron-atom potential energy

$$V_{\mathrm{ex}}=\frac{1}{2}(E-V_s)-\frac{1}{2}[(E-V_s)^2+4\pi\rho e^2\hbar^2/m]^{1/2}, \quad (10)$$

where E is the electron energy, V_s is the electrostatic scalar potential energy, ρ is the atomic electron density (obtained by Poisson's equation), and e is the electron charge.

4. Solid-state effects

When the target atom is bound in a solid, the outer electronic orbitals of the atom are modified. In order to take into account such a change, solid-state effects should be introduced. To describe solid-state effects, the muffin-tin model can be used in which the potential of each atom of the solid is altered by the nearest-neighbor atoms. Indicating with r_{ws} the radius of the Wigner-Seitz sphere and assuming that the nearest-neighbor atom is located at a distance $2r_{\mathrm{ws}}$, we may write the resulting potential

$$V_{\mathrm{solid}}(r)=V(r)+V(2r_{\mathrm{ws}}-r)-2V(r_{\mathrm{ws}}), \quad (11)$$

for $r<r_{\mathrm{ws}}$, and set it equal to zero elsewhere.

The term $2V(r_{\mathrm{ws}})$, introduced in order to shift the energy scale so that $V_{\mathrm{solid}}(r)=0$ at $r\geq r_{\mathrm{ws}}$ has also to be subtracted from the kinetic energy of the incident electron.[26]

5. Compound materials

The differential-elastic-scattering cross section, in molecular solids, can be approximated, by using the additivity rule,[31] as the sum of the atomic differential-elastic-scattering cross sections of all atoms in the molecule.

For example,

$$\left(\frac{d\sigma}{d\Omega}\right)_{\mathrm{SiO_2}}=\left(\frac{d\sigma}{d\Omega}\right)_{\mathrm{Si}}+2\left(\frac{d\sigma}{d\Omega}\right)_{\mathrm{O}}. \quad (12)$$

A more accurate approach consists in calculating the molecular differential-elastic-scattering cross sections. The computational procedure requires, in this case, the calculation of the coherent superposition of the waves scattered by the atoms constituting the molecule.

In our Monte Carlo calculations, however, we used the additivity rule; in order to test its accuracy we compared our calculation using this rule to experimental data and found very good agreement (see Fig. 2).

6. Total and transport cross section

Once the differential-elastic-scattering cross section is known, the calculation of the total-elastic-scattering cross section, σ_{el}, and of the momentum transfer (or transport) cross section, σ_{tr}, may be performed by the following equations:

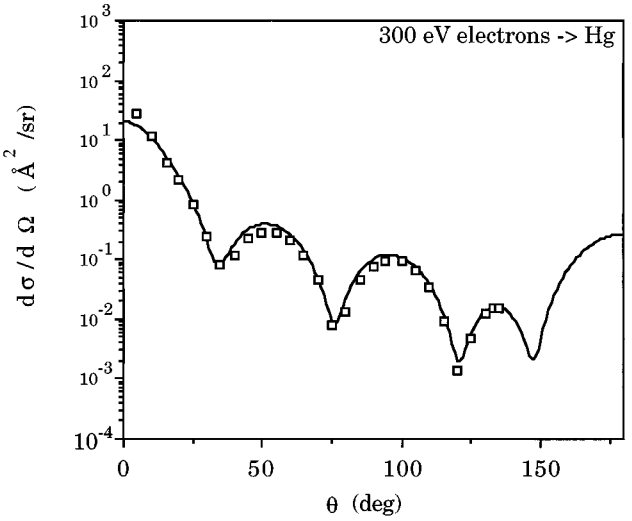

FIG. 1. Differential-elastic-scattering cross section of 300 eV electrons in Hg. Solid line: numerical computation. Squares: Holtkamp *et al.* (Ref. 67) experimental data.

$$\sigma_{\mathrm{el}}=2\pi\int_0^{\pi}\frac{d\sigma}{d\Omega}\sin\theta d\theta, \quad (13)$$

$$\sigma_{\mathrm{tr}}=2\pi\int_0^{\pi}(1-\cos\theta)\frac{d\sigma}{d\Omega}\sin\theta d\theta. \quad (14)$$

B. Inelastic scattering

1. Inelastic mean free path

Several numerical approaches were proposed in the literature, in recent years, to calculate the inelastic mean free path, λ_{inel}.[36–48] It is given by (see, for example, Ashley, Ref. 44):

$$\lambda_{\mathrm{inel}}^{-1}=\int p(E,\omega)d\omega, \quad (15)$$

with integration extended over all the allowed values of the energy transfer, ω. Here $p(E,\omega)$ is the probability for energy loss ω, per unit distance traveled by an electron of energy E. If q is the momentum transfer and $\epsilon(q,\omega)$ is the complex dielectric function describing the response of the medium, assumed homogeneous and isotropic, then $p(E,\omega)$ is given by[44]

$$p(E,\omega)=\frac{me^2}{\pi\hbar^2E}\int_{K_1}^{K_2}\frac{dq}{q}\mathrm{Im}\left[\frac{-1}{\epsilon(q,\omega)}\right], \quad (16)$$

where

$$K_1=\frac{\sqrt{2m}}{\hbar}(\sqrt{E}-\sqrt{E-\omega}), \quad (17)$$

and

$$K_2=\frac{\sqrt{2m}}{\hbar}(\sqrt{E}+\sqrt{E-\omega}). \quad (18)$$

TABLE I. Differential-elastic-scattering cross section (Å^2/ sr) of 1000 eV electrons impinging on Al.

θ (deg)	Fink and Ingram (Ref. 16)	Riley *et al.* (Ref. 18)	Salvat and Mayol (Ref. 26)	Present potential: Ref. 62	Present potential: Ref. 63
10	2.28	2.29	2.40	2.31	2.40
20	0.328	0.329	0.332	0.323	0.332
30	0.106	0.107	0.103	0.105	0.103
40	0.0468	0.0471	0.0457	0.0465	0.0457
50	0.0258	0.0260	0.0252	0.0259	0.0252
60	0.0168	0.0169	0.0160	0.0167	0.0160
70	0.0121	0.0122	0.0114	0.0121	0.0114
80	0.00945	0.00949	0.00886	0.00941	0.00886
90	0.00776	0.00778	0.00733	0.00771	0.00733
100	0.00664	0.00663	0.00637	0.00658	0.00637
110	0.00586	0.00584	0.00576	0.00579	0.00576
120	0.00530	0.00528	0.00535	0.00523	0.00535
130	0.00490	0.00488	0.00508	0.00483	0.00508
140	0.00461	0.00458	0.00490	0.00454	0.00490
150	0.00440	0.00437	0.00479	0.00433	0.00479
160	0.00426	0.00424	0.00471	0.00419	0.00471
170	0.00418	0.00416	0.00467	0.00411	0.00467

Ashley[43,44] has shown that, through second-order terms in $a=(\omega'/E)$, λ_{inel} may be computed by the following equation:

$$\lambda_{\text{inel}}^{-1}=\frac{me^2}{2\pi\hbar^2E}\int_0^{E/2}\text{Im}\left[\frac{-1}{\epsilon(0,\omega')}\right]L_e\left(\frac{\omega'}{E}\right)d\omega', \qquad (19)$$

where

$$L_e(a)=(1-a)\ln\frac{4}{a}-\frac{7}{4}a+a^{3/2}-\frac{33}{32}a^2. \qquad (20)$$

2. Stopping power

An electron can lose a large fraction of its energy in a single collision: nevertheless the continuous-slowing-down approximation is often used. In this approximation the electron is assumed to continuously dissipate its energy during its travel inside the solid. Thus we need an equation, or a tabulation, to express the rate of energy lost due to the electron-electron and electron-plasmon collisions.

The continuous-slowing-down approximation neglects the fluctuations of the energy-loss around its mean value. The energy-loss distribution, described by energy straggling parameters, is thus sometimes included in the simulations of the electron travel inside the solid.

When the electron energy is greater than 10 keV, energy losses are dominated by excitations and ionizations of the core electrons. In that case the stopping power, namely, the rate of energy loss per unit length, is well described by the Bethe-Bloch expression[49]

$$-\frac{dE}{ds}=\frac{2\pi e^4NZ}{E}\ln\left(\frac{1.166E}{J}\right), \qquad (21)$$

where J is the mean-atomic ionization energy[65,66] and N is the number of atoms per unit volume in the target.

The Bethe-Bloch stopping power does not work well when the electron energy becomes lower than J. To be more precise, it reaches a maximum for $E\approx 2.5J$ and then goes to zero for $E=J/1.166$. Below this energy value, the predicted stopping power becomes negative.

Kanaya and Okayama,[50] Rao-Sahib and Wittry,[51] Fitting[52] and, recently, Joy and Luo[59] proposed various semiempirical expressions to describe the electron energy loss per unit path length. Semiempirical expressions may be useful because they permit us to quickly calculate electron energy loss when computer time-consuming calculations are involved (for example in Monte Carlo codes). On the other hand, the semiempirical expressions are also inaccurate when the electron energy is very low ($E \lesssim 500$ eV).

In recent years, many accurate numerical results have been proposed by a number of authors in connection both with the stopping power and with inelastic mean free path.[36–39,43,44,55–58,61]

The stopping power is given by (see Ashley, Refs. 43,44)

$$-\frac{dE}{ds}=\int \omega p(E,\omega)d\omega, \qquad (22)$$

TABLE II. Total elastic-scattering cross section (Å^2) of electrons impinging on Ar atoms.

E_0 (eV)	Jansen *et al.* (Ref. 68)	DuBois and Rudd (Ref. 69)	Iga *et al.* (Ref. 70)	Present
50		7.17	-	7.38
100	3.81	4.79		4.32
200	3.02	3.05		3.05
400			2.13	2.20
500	1.99	2.02	1.71	1.97
800		1.35	1.31	1.52
1000			1.35	1.34

TABLE III. Total elastic-scattering cross section ($Å^2$) of electrons impinging on Hg atoms.

E_0 (eV)	Holtkamp *et al.* (Ref. 67)	Present
100	8.99	8.64
150	7.95	7.24
300	4.93	4.72

with integration extended over all the allowed values of the energy transfer ω.

$-dE/ds$ may be computed, through second-order terms in $a=(\omega'/E)$, by the following equation (see Ashley, Refs. 43,44):

$$-\frac{dE}{ds}=\frac{me^2}{\pi\hbar^2E}\int_0^{E/2}\mathrm{Im}\left[\frac{-1}{\epsilon(0,\omega')}\right]G_e\left(\frac{\omega'}{E}\right)\omega'\,d\omega', \quad (23)$$

where

$$G_e(a)=\ln\frac{1.166}{a}-\frac{3}{4}a-\frac{a}{4}\ln\frac{4}{a}+\frac{1}{2}a^{3/2}-\frac{a^2}{16}\ln\frac{4}{a}-\frac{31}{48}a^2. \quad (24)$$

In Monte Carlo simulations, when tabulations are used, the stopping power data must be interpolated by using, for example, cubic-spline interpolation. Also for the stopping power it is possible to use the additivity rule (Bragg's rule).[9]

III. RESULTS AND DISCUSSION

A. Elastic scattering

Figure 1 shows the comparison of our theoretical calculations, obtained by Eqs. (1)–(3) and (5) after numerical solution of the Dirac equation (7) [with the partial wave expansion method (PWEM)], to the experimental data of Holtkamp *et al.*[67] concerning differential-elastic-scattering cross section of 300-eV electrons in Hg: the introduction of the exchange effects in the atomic potential improves the accuracy of the calculation for the low-angle differential-elastic-scattering cross section so that the agreement between calculations and experiment is excellent at all the scattering angles. A comparison of the present calculation to numerical results of other authors concerning the differential electron elastic-scattering cross section in Al is given in Table I. The present calculation has been performed by using both the atomic potential of Cox and Bonham[62] and of Salvat *et al.*[63] Exchange and solid-state effects were included.

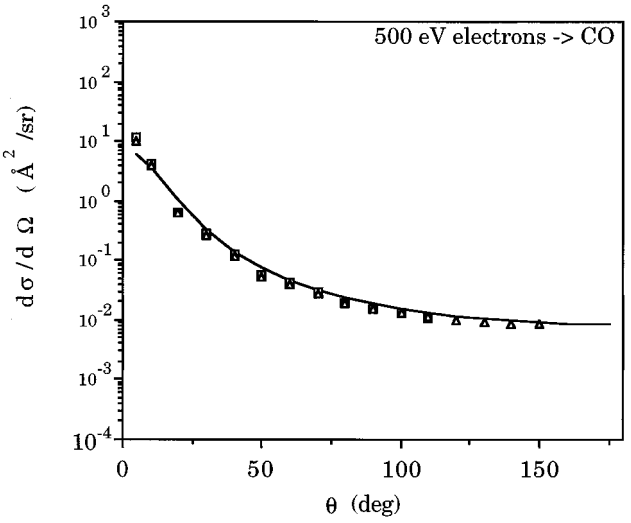

FIG. 2. Differential-elastic-scattering cross section of 500 eV electrons in CO. Solid line: numerical computation. Squares: Bromberg (Ref. 71) experimental data. Triangles: DuBois and Rudd (Ref. 69) experimental data.

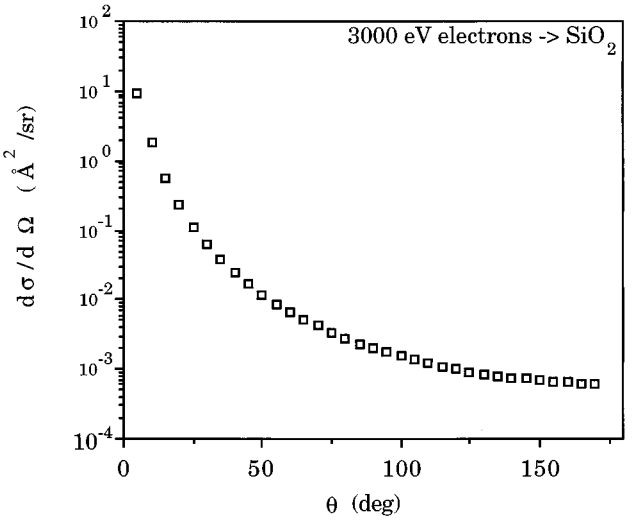

FIG. 3. Differential-elastic-scattering cross section of 3000 eV electrons in SiO_2. Numerical calculation.

The good accuracy of the calculation of the low-energy differential-elastic-scattering cross section, also at low angle of scattering, is reflected in the total-elastic-scattering cross section computation: In Tables II and III the experimental electron-atom total scattering cross sections as reported by Jansen *et al.*,[68] DuBois and Rudd,[69] Iga *et al.*[70] and Holtkamp *et al.*[67] are compared to our theoretical computations (PWEM). The agreement is satisfactory even for electron energies lower than 100 eV.

In order to test the additivity rule, we compared our results to the Bromberg[71] and the DuBois and Rudd[69] experi-

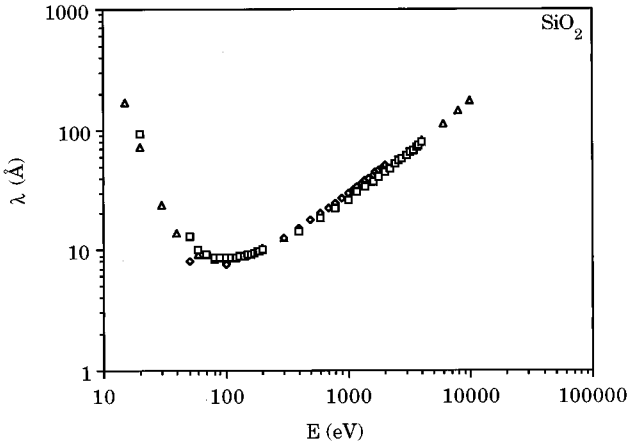

FIG. 4. Inelastic mean free path of electrons in SiO_2. Empty squares: Present. Triangles: Ashley and Anderson (Ref. 39). Rhombs: Tanuma, Powell, and Penn (Ref. 46).

TABLE IV. Comparison between elastic and inelastic mean free paths of low-energy electrons impinging on SiO_2.

E (eV)	λ_{el} Å	λ_{inel} Å	p_{inel}
50	3.17	12.9	0.20
100	4.55	8.49	0.35
1000	17.2	26.4	0.39
2000	29.0	44.7	0.39
3000	40.5	61.8	0.40
4000	51.6	78.1	0.40

mental data for the differential-elastic-scattering cross section of 500 eV electrons impinging on CO molecules: this comparison is presented in Fig. 2. The agreement is very good.

As a consequence, in the case of solid SiO_2, we used the additivity rule to calculate the differential and total elastic-scattering cross sections after including, in the atomic potential of the Si atoms, the solid-state effects described in Sec. II A 4 (the muffin-tin model). These numerical calculations are used in our Monte Carlo code that will be described in the following paper[5] for the evaluation of the backscattering and of depth distribution of the trapped electrons in SiO_2. In Fig. 3 our calculations, concerning the differential-elastic-scattering cross section of 3000 eV electrons impinging on SiO_2, are presented.

B. Inelastic scattering

Figure 4 shows the results of our numerical computation [Eqs. (19) and (20)] of the inelastic mean free path of low-energy electrons impinging on SiO_2 compared to the numerical results of Ashley and Anderson[39] and to those of Tanuma *et al.*[46] The energy-loss function of SiO_2, $\mathrm{Im}\{-[1/\epsilon(0,\omega)]\}$, was obtained from the tabulations of Henke *et al.*[72] for energies greater than 100 eV while, for energies lower than 40 eV, we used the experimental data of Buechner.[73] A linear interpolation was used for energies between 40 and 100 eV. The integration was performed by using the Bode rule[74] on a cubic-spline interpolation of the energy-loss function multiplied by $L_e(\omega'/E)$.

A comparison of our calculated inelastic and elastic mean free paths of electrons in SiO_2 was presented in Table IV. It is interesting to observe that the probability of inelastic scattering defined by

$$p_{\mathrm{inel}}=\frac{\lambda_{\mathrm{inel}}^{-1}}{\lambda_{\mathrm{inel}}^{-1}+\lambda_{\mathrm{el}}^{-1}} \tag{25}$$

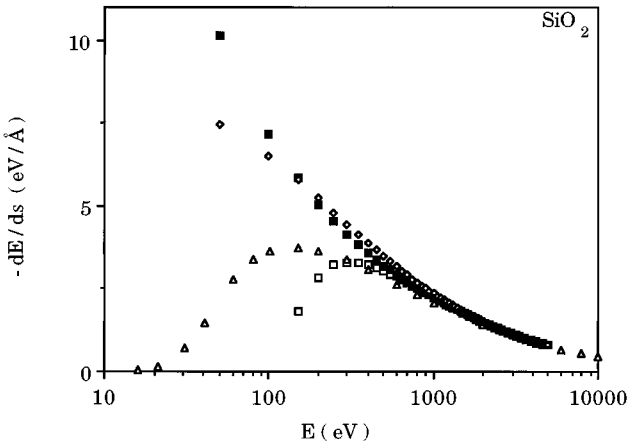

FIG. 5. Stopping power of electrons in SiO_2. Empty squares: Bethe (Ref. 49). Filled squares: Rao-Sahib and Wittry (Ref. 51). Triangles: Ashley and Anderson (Ref. 39). Rhombs: Joy and Luo (Ref. 59).

reaches a constant value of ≈ 0.40 for energies higher than ≈ 1000 eV (here $\lambda_{\mathrm{el}}^{-1}=N\sigma_{\mathrm{el}}$).

Figure 5 shows a comparison of stopping powers of electrons in SiO_2 computed with different formulas and numerical procedures that can be found in the literature. The different calculations give results which are in agreement for energies higher than 500 eV, while as expected, for very low kinetic energy there are great differences thus confirming the necessity to better understand the basic physical aspects involved in low-energy electron scattering with atoms and solids.

IV. CONCLUSION

We have analyzed the problem of the scattering process of low-energy electrons impinging on SiO_2, by calculating the elastic and inelastic contributions to the scattering event. To perform such a calculation, for low-energy electrons, we have carefully considered various approaches, both analytical and numerical; this analysis was necessary because, just in the low-energy scattering processes, there is no consolidated general formalism.

The numerical results, presented in this paper, were compared to experimental or computed results reported by other authors to show the validity of our approximations. The reported results form now the basis for treating the problem of the charging effects in insulators, during electron irradiation, a subject which will be developed in the following paper[5] and which is relevant, for example, in Auger analysis of dielectric solids.

[1] A. Miotello, Phys. Lett. **103A** 279 (1984).
[2] J. Cazaux, J. Appl. Phys. **59**, 1418 (1986).
[3] H. Chen, H. Gong, and C. K. Ong, J. Appl. Phys. **78**, 3714 (1995).
[4] A. Melchinger and S. Hofmann, J. Appl. Phys. **78**, 6224 (1995).
[5] A. Miotello and M. Dapor, following paper, Phys. Rev. B **56**, 2241 (1997).
[6] H. Niedrig, J. Appl. Phys. **53**, R15 (1982).
[7] J. I. Goldstein, D. E. Newbury, P. Echlin, D. C. Joy, and C. Fiori, *Scanning Electron and X-Ray Microanalysis* (Plenum, New York, 1984), pp. 53–122.
[8] D. E. Newbury, D. C. Joy, P. Echlin, C. E. Fiori, and J. I. Goldstein, *Advanced Scanning Electron Microscopy and X-Ray Mi-*

croanalysis (Plenum, New York, 1986), pp. 3–43.
[9] L. C. Feldman and J. W. Mayer, *Fundamentals of Surface and Thin Film Analysis* (North-Holland, New York, 1986), pp. 125–153.
[10] G. Messina, A. Paoletti, S. Santangelo, and A. Tucciarone, Riv. Nuovo Cimento **15**, 1 (1992).
[11] N. F. Mott, Proc. R. Soc. London **124**, 425 (1929).
[12] S. -R. Lin, N. Sherman, and J. K. Percus, Nucl. Phys. **45**, 492 (1963).
[13] P. J. Bunyan and J. L. Schonfelder, Proc. Phys. Soc. London **85**, 455 (1965).
[14] N.F. Mott and H.S.W. Massey, *The Theory of Atomic Collisions* (Oxford University Press, New York, 1965), pp. 210–258.
[15] M. Fink and A. C. Yates, At. Data **1**, 385 (1970).
[16] M. Fink and J. Ingram, At. Data **4**, 129 (1972).
[17] D. Gregory and M. Fink, At. Data Nucl. Data Tables **14**, 39 (1974).
[18] M. E. Riley, C. J. MacCallum, and F. Biggs, At. Data Nucl. Data Tables **15**, 443 (1975).
[19] F. Salvat, R. Mayol, and J. D. Martinez, J. Phys. B **20**, 6597 (1987).
[20] I. S. Tilinin, Zh. Eksp. Teor. Fiz. **94**, 96 (1988) [Sov. Phys. JETP **67**, 1570 (1988)].
[21] D. Liljequist, M. Ismail, F. Salvat, R. Mayol, and J. D. Martinez, J. Appl. Phys. **68**, 3061 (1990).
[22] Z. Czyzewski, D. O'Neill MacCallum, A. Romig, and D. C. Joy, J. Appl. Phys. **68**, 3066 (1990).
[23] A. Jablonski, Phys. Rev. B **43**, 7546 (1991).
[24] W. S. M. Werner, J. Electron Spectrosc. Relat. Phenom. **59**, 275 (1992).
[25] W. F. Egelhoff,Jr., Phys. Rev. Lett. **71**, 2883 (1993).
[26] F. Salvat and R. Mayol, Comput. Phys. Commun. **74**, 358 (1993).
[27] J. M. Fernández-Varea, R. Mayol, J. Baró, and F. Salvat, Nucl. Instrum. Methods Phys. Res. B **73**, 447 (1993).
[28] J. Kawata and K. Ohya, Nucl. Instrum. Methods Phys. Res. B **90**, 29 (1994).
[29] R. Szmytkowski and J. E. Sienkiewicz, Phys. Rev. A **50**, 4007 (1994).
[30] A. Jablonski and C. J. Powell, Phys. Rev. B **50**, 4739 (1994).
[31] J. Baró, J. Sempau, J. M. Fernández-Varea, and F. Salvat, Nucl. Instrum. Methods Phys. Res. B **100**, 31 (1995).
[32] M. Dapor, Nucl. Instrum. Methods Phys. Res. B **95**, 470 (1995); **108**, 363 (1996).
[33] M. Dapor, J. Appl. Phys. **77**, 2840 (1995).
[34] M. Dapor, J. Appl. Phys. **79**, 8406 (1996).
[35] M. P. Seah and W. A. Dench, Surf. Interface Anal. **1**, 2 (1979).
[36] J. C. Ashley, C. J. Tung, R. H. Ritchie, and V. E. Anderson, IEEE Trans. Nucl. Sci. **NS23**, 1833 (1976).
[37] J. C. Ashley, C. J. Tung, and R. H. Ritchie, Surf. Sci. **81**, 409 (1979).
[38] C. J. Tung, J. C. Ashley, and R. H. Ritchie, Surf. Sci. **81**, 427 (1979).
[39] J. C. Ashley and V. E. Anderson, IEEE Trans. Nucl. Sci. **NS28**, 4132 (1981).
[40] D. R. Penn, Phys. Rev. B **35**, 482 (1987).
[41] C. J. Powell, Surf. Interface Anal. **10**, 349 (1987).
[42] S. Tanuma, C. J. Powell, and D. R. Penn, Surf. Interface Anal. **11**, 577 (1988).
[43] J. C. Ashley, J. Electron Spectrosc. Relat. Phenom. **46**, 199 (1988).
[44] J. C. Ashley, J. Electron Spectrosc. Relat. Phenom. **50**, 323 (1990).
[45] S. Tanuma, C. J. Powell, and D. R. Penn, Surf. Interface Anal. **17**, 911 (1991).
[46] S. Tanuma, C. J. Powell, and D. R. Penn, Surf. Interface Anal. **17**, 927 (1991).
[47] S. Tanuma, C. J. Powell, and D .R. Penn, Surf. Interface Anal. **21**, 77 (1993).
[48] S. Tanuma, C. J. Powell, and D. R. Penn, Surf. Interface Anal. **21**, 165 (1993).
[49] H. A. Bethe, Ann. Phys. (Leipzig) **5**, 325 (1930).
[50] K. Kanaya and S. Okayama, J. Phys. D **5** 43 (1972).
[51] T. S. Rao-Sahib and D. B. Wittry, J. Appl. Phys. **45**, 5060 (1974).
[52] H. -J. Fitting, Phys. Status Solidi A **26**, 525 (1974).
[53] G. Love, M. G. Cox, and V. D. Scott, J. Phys. D **11**, 7 (1978).
[54] J. Schou, Phys. Rev. B **22**, 2141 (1980).
[55] F. Salvat, J. D. Martinez, R. Mayol, and J. Parellada, J. Phys. D **18**, 299 (1985).
[56] R. Mayol, J. D. Martinez, and F. Salvat, Nucl. Instrum. Methods Phys. Res. A **255**, 117 (1987).
[57] R. M. Nieminen, Scanning Microsc. **2**, 1917 (1988).
[58] Z. -J. Ding and R. Shimizu, Surf. Sci. **222**, 313 (1989).
[59] D. C. Joy and S. Luo, Scanning **11**, 176 (1989).
[60] P. M. Echenique and A. Arnau, Phys. Scr. **T49B**, 677 (1993).
[61] A. Akkerman, T. Boutboul, A. Breskin, R. Chechik, A. Gibrekhterman, and Y. Lifshitz, Phys. Status Solidi B **198**, 769 (1996).
[62] H. L. Cox, Jr. and R. A. Bonham, J. Chem. Phys. **47**, 2599 (1967).
[63] F. Salvat, J. D. Martínez, R. Mayol, and J. Parellada, Phys. Rev. A **36**, 467 (1987).
[64] J. B. Furness and I. E. McCarthy, J. Phys. B **6**, 2280 (1973).
[65] M. J. Berger and S. M. Seltzer, National Research Publication 1133, Washington D.C. (1964) p. 205.
[66] ICRU Report 37, 1984 (unpublished).
[67] G. Holtkamp, K. Jost, F. J. Petzman, and J. Kessler, J. Phys. B **20**, 4543 (1987).
[68] R. H. J. Jansen, F. J. de Heer, H. J. Luyken, B. van Wingerden, and H. J. Blaauw, J. Phys. B **9**, 185 (1976).
[69] R. D. DuBois and M. E. Rudd, J. Phys. B **9**, 2657 (1976).
[70] I. Iga, L. Mu-Tao, J. C. Nogueira, and R. S. Barbieri, J. Phys. B **20**, 1095 (1987).
[71] J. P. Bromberg, J. Chem. Phys. **52**, 1243 (1970).
[72] B. L. Henke, P. Lee, T. J. Tanaka, R. L. Shimabukuro, and B. K. Fujikawa, At. Data Nucl. Data Tables **27**, 1 (1982).
[73] U. Buechner, J. Phys. C **8**, 2781 (1975).
[74] S. E. Koonin and D. C. Meredith, *Computational Physics* (Addison-Wesley, New York, 1990), pp. 6–11.